THE ASTROPHYSICAL JOURNAL, 495:609–616, 1998 March 10

A REALISTIC GRID OF MODELS FOR THE GRAVITATIONALLY LENSED EINSTEIN CROSS (Q2237+0305) AND ITS RELATION TO OBSERVATIONAL CONSTRAINTS

KYU-HYUN CHAE, DAVID A. TURNSHEK, AND VALERY K. KHERSONSKY
Department of Physics and Astronomy, University of Pittsburgh, Pittsburgh, PA 15260
Received 1997 March 27; accepted 1997 October 20

ABSTRACT

A detailed study of a power-law lens model is presented for the gravitational lens system Q2237+0305, also known as the Einstein Cross. The adopted three-dimensional distribution for the mass of the lens is more realistic than in previous models and is described by $\rho(X, Y, Z) = \rho_0[1 + (X/a)^2 + (Y/b)^2 + (Z/c)^2]^{-\nu/2}$. *Hubble Space Telescope* (*HST*) optical positions of the image components and the center of the galactic bulge (Crane et al.) along with radio flux density ratios of the image components (Falco et al.) are used to constrain the model [8 (four relative optical positions) + 3 (relative magnifications) = 11 constraints]. The goodness of fit χ^2 is defined using these constraints. The best model has $\chi^2 \approx 14$, which is a better fit than all previous models. We investigate the characteristics of models within the 99% confidence region of parameter space around the best model. We find that the lensing properties (i.e., total image magnification, relative image magnifications, and time delays between image pairs) of models are well described by the ellipticity of the projected mass of the lens, and we calculate a grid of models that illustrates how the lensing properties depend on the ellipticity. We discuss how future observations, such as placing tighter constraints on the brightness of any fifth image, can be used to further constrain the grid of models presented here. The possibility of using the grid of models to place constraints on the Hubble constant is also discussed.

Subject headings: gravitational lensing — quasars: individual (Q2237+0305, Einstein Cross)

1. INTRODUCTION

The gravitational lens system Q2237+0305 was discovered by Huchra et al. (1985) in the CfA Redshift Survey of Galaxies. Four bright images of a distant QSO ($z \approx 1.695$) are superposed on a nearby barred spiral galaxy ($z \approx 0.039$). Because of its proximity, the properties of the lensing galaxy have been studied in more detail than in any other lensed systems (e.g., Yee 1988; Racine 1991; Rix, Schneider, & Bahcall 1992).

Two different approaches have been applied to model this system: (1) a constant mass-to-light ratio approach and (2) a multiparametric approach. The constant mass-to-light ratio method was first adopted by Schneider et al. (1988). By assuming that the observed light distribution of the galaxy was proportional to the projected mass distribution, they found that the observed image positions could be qualitatively explained. Later, Rix et al. (1992) obtained a more accurate light distribution for the lensing galaxy using *Hubble Space Telescope* (*HST*) Wide Field Camera observations. The Rix et al. (1992) model reproduced the observed image positions to an accuracy $\approx 0\farcs03$. However, this is still significantly larger than the observational uncertainty ($\lesssim 0\farcs015$; Rix et al. 1992). The discrepancies indicated that the constant mass-to-light ratio model was not a very accurate description of the lens, although it qualitatively explained the observed image properties and was simple enough to have only three free parameters (mass-to-light ratio, x and y positions of the QSO on the source plane). In fact, there is no a priori reason that the shape of the light distribution should be *quantitatively* representative of that of the mass distribution in the spiral galaxy, especially since the dark halo mass distribution is less flattened than the light distribution. In terms of ellipticity, we do not expect that the ellipticity of the mass is identical to that of the light. Thus, it would be better to allow the ellipticity to be a free parameter in the lens modeling and determine its value, consistent with observational constraints (i.e., image geometry and magnification ratios). For further consideration of the relationship between the shapes of the mass and the light in lensing galaxies the reader is referred to Keeton, Kochanek, & Seljak (1997) and Keeton & Kochanek (1998).

Multiparametric models have been achieving better agreement with observed image positions. There have been two conceptually different methods in the multiparametric approach. One method was to model the mass distribution of the galaxy with elliptical mass densities. For example, Kent & Falco (1988) considered a de Vaucouleurs law and a King profile mass distribution. At the time they reproduced the image positions within the observational uncertainty of the best available data (Yee 1988). The other method was to use a shear, γ, to account for the ellipticity, while using a spherically symmetrical lens as the dominant contribution. Kochanek (1991) used a singular isothermal sphere and a point mass along with different types of shear (internal, external, and mixed). Wambsganss & Paczyński (1994, hereafter WP94) used a singular power-law sphere with an external shear; the mass distribution was $M(r) \sim r^{\beta}$ ($0 \leq \beta < 2$) with an external shear γ.

In 1991 two groups reported more accurate observations of the system. Crane et al. (1991, hereafter C91) used the *HST* Faint Object Camera to derive positions with a formal error of $0\farcs005$ along with photometric results. Racine (1991) used Canada-France-Hawaii Telescope (CFHT) images to derive positions and relative magnitudes to an accuracy $0\farcs002$ and 0.01 mag, respectively. Furthermore, he reported evidence for a fifth image (which he called component "E") close to the center of the galaxy ($0\farcs07 \pm 0\farcs035$ south-southeast of the galaxy's center) that was 4.5 ± 0.3 mag fainter than component A. WP94 used only the new positions of C91 as model constraints. Their model reproduced the image positions to an accuracy better than $0\farcs01$ (2 σ).

WP94's calculated relative magnifications of the images were almost the same for values of β in the range $0.0 \leq \beta \leq 1.85$, probably because of the lens astigmatism (see WP94). In other words, based on their predictions for the image positions and relative magnifications, WP94's models from a point lens ($\beta = 0$) up to a nearly constant surface density lens ($\beta \approx 2$) were almost indistinguishable (see § 4). The total magnification ranged from 8 to more than 1000, and the maximum time delay (τ_{CB} between components C and B) ranged from greater than 20 h_{75}^{-1} hr to 1.5 h_{75}^{-1} hr for $0.0 \leq \beta \leq 1.85$. This means that even if WP94's predicted relative image magnifications were consistent with observations, we could not use them to constrain the magnifications or time delays. In fact, however, the current observed estimate of R_{DA} (relative magnification of component D with respect to A) implies that WP94's models may not be consistent with the observations (see below).

While the observed image positions have been reproduced with good accuracy (0.″007–0.″01) by WP94, up to now two other important properties of the Einstein Cross have not been investigated in quantitative detail. First, it is not clear whether existing models are consistent with the image brightness ratios. In previous modeling attempts it was realized that the mismatch between theoretical image magnification ratios and observed optical brightness ratios is partly due to dust extinction and microlensing effects in the optical images. This is why all of the previous models placed most of the emphasis on modeling the observed image positions. Falco et al. (1996, hereafter F96) reported on VLA observations of the system. The radio images showed a flat spectrum source detected with a total flux density of $\approx$0.7 mJy at 20 cm and 3.6 cm. The measured radio image positions (with uncertainties $\sigma \approx 0.''02$) were in excellent agreement with the optical image positions (C91) to within their uncertainties. However, the measured radio flux density ratios were different from the optical image brightness ratios (e.g., Racine 1991). The brightness ratio R_{DA} was significantly larger in the radio. The radio flux density ratios are more likely to represent the macrolensing image magnifications (see § 4). The most successful model to date in matching the observed image positions (WP94) is only roughly consistent with the observed radio flux density ratios. In particular, the observed radio flux density ratio of component D with respect to component A is $R_{DA} = 0.77 \pm 0.23$ (F96) and WP94's expected R_{DA} lies between $\approx$0.98 and 1.15. Secondly, while evidence for a fifth image has been reported (Racine 1991; Rix et al. 1992), the previous models for the Einstein Cross either did not take into account or could not predict a fifth image. For example, WP94 considered singular models that do not allow a fifth image.

In this paper we calculate a simple but realistic grid of gravitational lens models for the Einstein Cross. The basic model directly considers the three-dimensional distribution of mass in the lensing galaxy. A brief description of the basic model is given in § 2, and the details of the model can be found in Chae, Khersonsky, & Turnshek (1998, hereafter CKT) and in Chae (1998). Our best models can reproduce the observed image positions (C91) to an accuracy rms $\approx$ 0.″006 with component A fixed (rms $\approx$ 0.″0054 with component A varied and can be compared to the WP94 best agreement of 0.″007), better agreement than in all previous models. Our models predict a wide range of image magnifications depending mostly on the ellipticity of the projected mass. This suggests that if the image magnification ratios can be well constrained by observations, then this can in turn be used to deduce the best power-law model for the Einstein Cross with corresponding ellipticity. We also quantify the relation between the lens core size and the relative brightness of the fifth image for the Einstein Cross. For a detailed study on the relation between the core radius and the fifth image brightness of a lens the reader is referred to Wallington & Narayan (1993). Our results are summarized in § 3. We discuss the implications of the results in § 4.

2. A BRIEF DESCRIPTION OF THE TRIAXIAL MODEL OF MASS DISTRIBUTION

We adopt the power-law (nonsingular) density for the distribution of mass in a galaxy (CKT),

$$\rho(X, Y, Z) = \rho_0 \left[1 + \left(\frac{X}{a}\right)^2 + \left(\frac{Y}{b}\right)^2 + \left(\frac{Z}{c}\right)^2 \right]^{-\nu/2}, \quad (1)$$

where (X, Y, Z) are the body coordinates attached to the galaxy. The parameter ρ_0 is the density at the center of the galaxy; ν is the radial index of the mass distribution; and (a, b, c) are the scale parameters along each axis (i.e., lens core sizes), where $a \geq b \geq c$ by convention. The case of $\nu = 2$ is called an "isothermal" distribution. The mass inside $r = (X^2 + Y^2 + Z^2)^{1/2}$ scales asymptotically as $M(r) \sim r^{3-\nu}$ for $1 < \nu < 3$. We note that the parameter ν is related to the parameter η in the model by Grogin & Narayan (1996) through $3 - \nu = \eta$ $(0 < \eta < 2)$.

Since gravitational lensing is governed by the projected surface mass density on the sky (i.e., the lens plane) and the galaxy can be oriented in an arbitrary fashion relative to the lens plane, three additional parameters are needed to relate the body coordinates (X, Y, Z) to the lens coordinates (x, y, z) where z is the direction toward the observer. They are the Eulerian angles (α, β, γ).[1] The parameters (α, β, γ) have the following geometrical meanings. Consider the intersection between the X-Y plane of the body and the lens plane, which is known as the line of nodes (e.g., see Goldstein 1980). The parameter α is the angle between the X-axis of the body and the line of nodes in the counterclockwise direction on the X-Y plane around the Z-axis. Note that if $a = b$, the parameter α has no effect. The parameter β is the angle between the Z-axis of the body and the z-axis of the lens coordinates in the counterclockwise direction around the line of nodes. The parameter β is thus an inclination angle such that $\beta = 0$ is face-on. The parameter γ is the angle between the line of nodes and the x-axis of the lens coordinates in the counterclockwise direction on the lens plane around the z-axis. If $a = b$, the parameter γ is related to the position angle (P.A., from the north to the east in the counterclockwise direction) via $\gamma = 90° - \text{P.A.}$

Now the distribution of mass on the lens plane takes the form

$$\Sigma(x, y) = \int_{-\infty}^{+\infty} \rho(x, y, z) dz = \frac{\Sigma_0}{(1 + c_x x^2 + c_y y^2 + c_{xy} xy)^{\mu+1}}, \quad (2)$$

where $\mu \equiv (\nu - 3)/2$. The case of $\mu = -\frac{1}{2}$ (or $\nu = 2$) and $c_{xy} = 0$ is the familiar isothermal surface density for which the lensing properties were studied in great detail by

[1] The symbols β and γ should not be confused with the mass exponent and external shear, respectively.

Kassiola & Kovner (1993) and Kormann, Schneider, & Bartelmann (1994). Especially, the singular isothermal densities (i.e., for $a \to 0$) were widely used both in modeling individual lenses (e.g., Ratnatunga et al. 1995; Keeton et al. 1997) and in statistical studies of lenses (e.g., Turner, Ostriker, & Gott 1984; Kochanek 1996). In polar coordinates equation (2) becomes

$$\Sigma(r, \phi) = \frac{\Sigma_0}{[1 + Pr^2 + Qr^2 \sin(2\phi + S)]^{\mu+1}}, \quad (3)$$

where $P = (c_x + c_y)/2$, $S = \tan^{-1}[(c_x - c_y)/c_{xy}]$, and $Q = (c_x - c_y)/(2 \sin S)$. The parameters (c_x, c_y, c_{xy}) (thus also P, Q, S) depend on (a, b, c) and (α, β, γ). The central surface density Σ_0 depends on ρ_0, μ, a, b, c and α, β. The complete expressions for these variables can be found in CKT and are not repeated in this paper. The ellipticity of the projected mass distribution is given by

$$\epsilon = 1 - q = 1 - \frac{r_{\min}}{r_{\max}} = 1 - \sqrt{\frac{1 - |Q|/P}{1 + |Q|/P}}, \quad (4)$$

where $r_{\min}$ and $r_{\max}$ are the semiminor and semimajor axes, respectively, in an ellipse of constant surface density on the lens plane. The complete analytic expressions for the deflection angle and image magnification factor calculated for the surface density given by equation (3) can be found in CKT.[2]

In the Einstein Cross, the lens is known to be a barred spiral galaxy. However, the bar, which could cause an asymmetry in the mass distribution, is extended much larger than the image separations, and so we ignore the bar. Therefore, assuming that the total mass distribution for the lensing is axisymmetric (see below and § 4), we set $a = b$ and define $\omega \equiv a/c(\omega > 1)$, i.e., ω is the major-to-minor axis ratio of an oblate ellipsoid. Noticing that the projected axis ratio q can be expressed in terms of ω and β (Keeton & Kochanek 1998) as follows

$$q = \left(\frac{1}{\omega^2} \sin^2 \beta + \cos^2 \beta\right)^{1/2}, \quad (5)$$

we see that there is a degeneracy between ω and β in the model. For this study we arbitrarily set $\beta = 60°$ and vary ω to change the ellipticity. Doing this allows the ellipticity to approach 0.5, although a 99% confidence level limits $\epsilon \lesssim 0.35$ (see § 3). If the true inclination angle is 60°, the fitted value of ω will represent the true model axis ratio. Otherwise, equation (5) can be used to infer the true axis ratio for the given value of the inclination angle. The inclination angle inferred from the observed light distribution of the optical disk ranges from $\beta = 45.^\circ6$ to $\beta = 64.^\circ5$ (see § 3). So in this model of the Einstein Cross the number of free parameters is seven: (1) the density at the center ρ_0, (2) the radial index v, (3) the core size a, (4) the major-to-minor axis ratio ω, (5) the angle γ, (6) and (7) the horizontal and vertical coordinates of the QSO on the source plane. A characteristic of our model is simplicity. We do not intend to model all of the individual mass components (i.e., bulge, disk, halo, and bar) of the galaxy, but assume that the mass density of equation (3) is a realistic representation of the total mass distribution.[3]

The goodness of fit χ^2 is defined as[4]

$$\chi^2 = \sum_i \left(\frac{x_{iA}^{\rm th} - x_{iA}^{\rm ob}}{\sigma_{x_{iA}}}\right)^2 + \sum_i \left(\frac{y_{iA}^{\rm th} - y_{iA}^{\rm ob}}{\sigma_{y_{iA}}}\right)^2 + \sum_j \left(\frac{R_{jA}^{\rm th} - R_{jA}^{\rm ob}}{\sigma_{R_{jA}}}\right)^2, \quad (6)$$

where i = B, C, D, G and j = B, C, D, with G denoting the galaxy's center. The parameters $x_{iA}^{\rm th}$ and $x_{iA}^{\rm ob}$ are the theoretical and observational relative horizontal positions (i.e., right ascensions), respectively, of components B, C, D, G with respect to component A. The parameters $y_{iA}^{\rm th}$ and $y_{iA}^{\rm ob}$ are the theoretical and observational relative vertical positions (i.e., declinations), respectively, of components B, C, D, G with respect to component A. The parameters $R_{jA}^{\rm th}$ and $R_{jA}^{\rm ob}$ are the theoretical and observational relative magnifications, respectively, of components B, C, D with respect to component A. Finally, $\sigma_{x_{iA}}$ and $\sigma_{y_{iA}}$ are the observational uncertainties in the positions, while $\sigma_{R_{jA}}$ is the observational uncertainty of the flux density ratios, all relative to component A.

The radial index v and core size a were fixed for each model, and all the other parameters were varied to minimize χ^2. The parameters v and a were incremented with step sizes of 0.02 and 0.01 h_{75}^{-1} kpc, respectively. The singular case ($a = 0$) was excluded from consideration. The lowest value considered for a was 0.01 h_{75}^{-1} kpc, but for $a \lesssim 0.02$ h_{75}^{-1} kpc the model has little dependence on a.

3. RESULTS

A standard cosmology with zero cosmological constant was assumed, and the calculation was done with $H_0 = 75$ km s^{-1} Mpc^{-1} and deceleration parameter $q_0 = \frac{1}{2}$. The parameter q_0 has little influence on any calculated quantities (e.g., relative magnifications) because the lens is so nearby. The Hubble constant has the effect of rescaling the parameter a and the calculated time delay τ according to H_0^{-1} (for $H_0 = 75\ h_{75}$ km s^{-1} Mpc^{-1}, $a \propto h_{75}^{-1}$, and $\tau \propto h_{75}^{-1}$).

We calculated $\approx$1000 models by incrementing the parameters v and a. Each of these models corresponds to a point on the grid of the two-dimensional parameter space spanned by v and a. A model with $v = 1.58$ and $a = 0.04$ h_{75}^{-1} kpc has the lowest value of χ^2 (eq. [6]), which is $\chi^2_{\min} \approx 14.13$. From now on this model will be referred to as the "best" model. The other parameters obtained for the best model are $\rho_0 = 2.482 \times 10^2\ M_\odot$ pc^{-3}, $\omega = 1.197$, $\gamma = 23.^\circ12$, and $\boldsymbol{x}_s = (0.1524, -0.0288)\ h_{75}^{-1}$ kpc (on the source plane). Figure 1 shows the image configuration of the best model.

Figure 2 shows confidence limits around the best model on the two-dimensional parameter space assuming a normal distribution (Press et al. 1992). Within a 99% con-

[2] The resulting expressions for the deflection and magnification are fast converging series.

[3] A detailed study of lensing by spiral galaxies can be found in Keeton & Kochanek (1998). They considered lens models consisting of halo, disk, and bulge components combined to produce a flat rotation curve.

[4] WP94 used a similar definition but without the additional constraint from the radio flux density ratios.

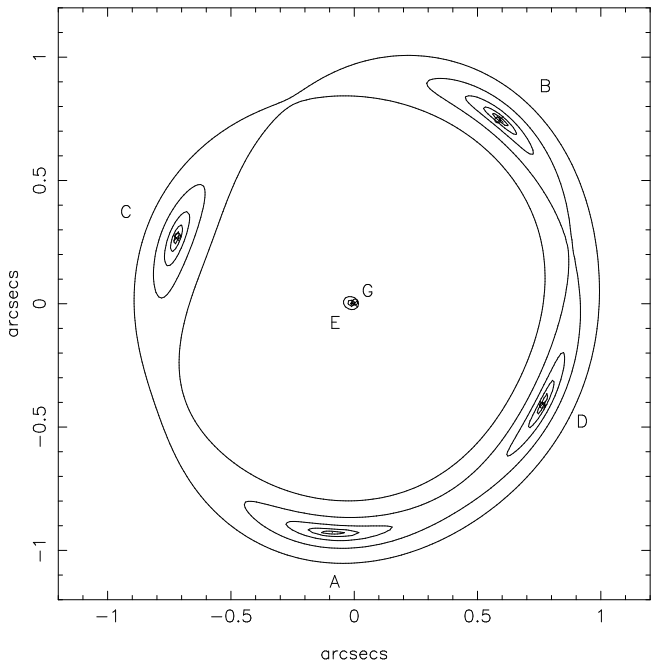

FIG. 1.—Image configuration of a model with $v = 1.58$ and $a = 0.04$ h_{75}^{-1} kpc, which is the best-fitting model. The five contour levels correspond to 25, 50, 100, 200, and 400 pc from the center of the QSO on the source plane. The small open circles are the observed *relative* positions of the components and the galaxy center (B, C, D, G) with respect to component A (C91). The radius of the circle corresponds to C91's 2 σ uncertainty (i.e., 0.″01). The center of the model lens is located at the origin and is marked by a cross. The centroids of the theoretical images (B, C, D) are also marked by a cross. The model predicts a fifth image at (−0.″0110, 0.″0025) from the origin.

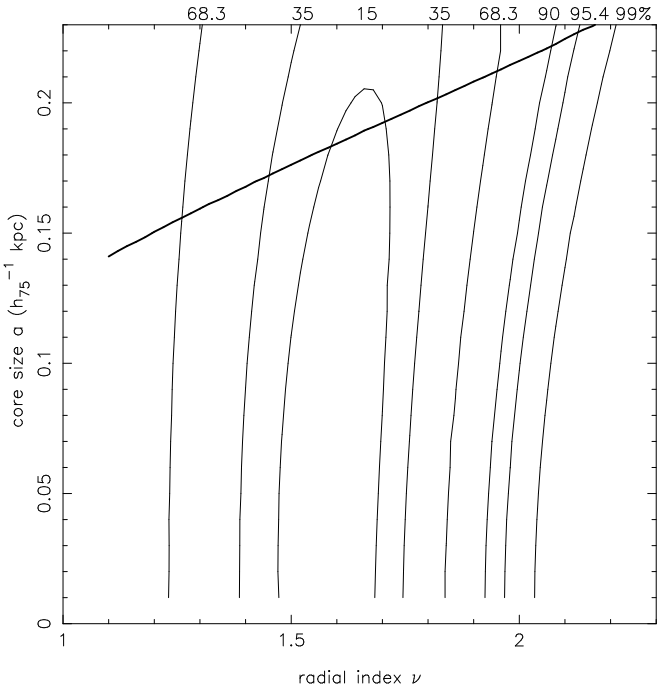

FIG. 2.—Distribution of χ^2 (i.e., the goodness of fit defined by eq. [6]) on the grid of two-dimensional parameter space spanned by v and a. The six ellipses representing confidence limits of 15%, 35%, 68.3%, 90%, 95.4%, and 99% from the best model are drawn. The radial index v of the density profile (eq. [1]) ranges from ≈ 1.1 to ≈ 2.3. Models with $v \approx 1.0$ were excluded from consideration (see § 3). Since models of large lens core sizes predict a bright fifth image, an upper limit on a was set by requiring $R_{EA} < 0.07$ for each v (see § 3). The thick line corresponds to core sizes for which $R_{EA} = 0.07$.

fidence limit χ^2 ranges from ≈ 14.1 to ≈ 23.3 (or, $\Delta\chi^2 = \chi^2 - \chi^2_{min}$ ranges from 0 to 9.21). Table 1 summarizes the ranges of model predictions within the 99% confidence limit. The upper limit on a for each v was set by requiring that R_{EA} (the relative brightness of component E with respect to component A) be less than 0.07. The thick line in Figure 2 represents core sizes for which $R_{EA} = 0.07$. The absolute lower limit on v is 1.0, which corresponds to a constant surface density. We excluded from consideration those models that were too close to $v = 1.0$ (i.e., $v < 1.1$)

Figure 3 shows the ϵ distribution of the models on the same grid of v and a. The ellipticity ϵ ranges from ≈ 0.01 to ≈ 0.35 within the 99% confidence limit. The best model has an ellipticity of $\epsilon = 0.12$. Models along each curve on Figure 3 have the same ellipticity. Most of the region of parameter space within the 99% confidence limit has lower ellipticities than the ellipticity of the observed light distribution. Huchra et al. (1985) obtained $\epsilon_{light} = 0.47$. Yee (1988) obtained a higher value of $\epsilon_{light} = 0.57$. Two more recent observations show that $\epsilon_{light} \approx 0.3$, namely, Racine (1991) obtained $\epsilon_{light} = 0.31 \pm 0.01$ using the CFHT data, and Rix et al. (1992) found $\epsilon_{light} = 0.3$ from *HST* Wide Field Camera observations. Using equation (5), we find that the above ellipticities of light are consistent with inclination angles of 45.°6 to 64.°5 for a thin galactic disk.

Our grid of models show that the characteristics of a model are well constrained by its ellipticity. Those models that have the same ellipticity (i.e., the set of points defining

TABLE 1

RANGE OF MODEL PREDICTIONS WITHIN A 99% CONFIDENCE LIMIT

Model Prediction	Range
Ellipticity	$0.01 \lesssim \epsilon \lesssim 0.35$
Total Magnification	$15 \lesssim \mathcal{M}_{total} \lesssim 4000$
Magnification of component B relative to component A	$0.88 \lesssim R_{BA} \lesssim 0.90$
Magnification of component C relative to component A	$0.45 \lesssim R_{CA} \lesssim 0.70$
Magnification of component D relative to component A	$0.78 \lesssim R_{DA} \lesssim 1.30$
Magnification of component E relative to component A	$0.0 \lesssim R_{EA} \lesssim 0.07$
Time delay for component A relative to component B (h_{75}^{-1} hr)	$0.13 \lesssim \tau_{AB} \lesssim 3.4$
Time delay for component C relative to component B (h_{75}^{-1} hr)	$0.90 \lesssim \tau_{CB} \lesssim 20$
Time delay for component D relative to component B (h_{75}^{-1} hr)	$0.35 \lesssim \tau_{DB} \lesssim 8.9$
Time delay for component E relative to component B (h_{75}^{-1} hr)	$1.9 \lesssim \tau_{EB} \lesssim 48$

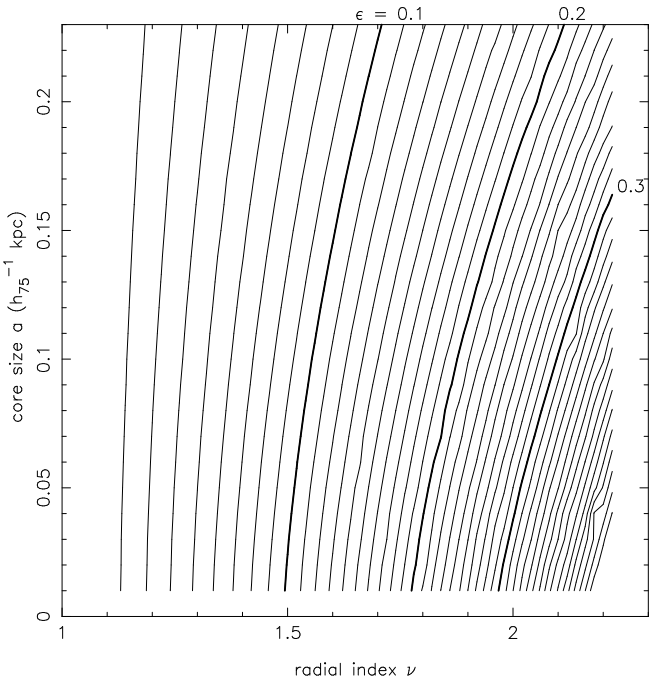

FIG. 3.—Distribution of ellipticity ϵ (defined by eq. [4]) on the same grid of two-dimensional parameter space as in Fig. 2. Each curve forms a set of models that have the same ϵ.

each curve on Fig. 3) predict similar total magnification, relative magnifications, and time delays. On the other hand, the relative magnification of component E depends on the core size a, as well as ϵ. In Figure 4 the dependence between the total magnification and the ellipticity is displayed. It is remarkable how dramatically the total magnification changes (from ≈ 15 to > 4000) as ϵ varies. Models of higher ellipticity predict smaller total magnifications. Although models of very large total magnifications are included within the 99% confidence limit with the given definition of χ^2, the Baldwin relationship—a weak correlation between the C IV emission line equivalent width and the luminosity of the QSO (Huchra et al. 1985)—suggests that it is unlikely for the total magnification to be larger than several tens, thereby favoring models of higher ellipticity.

The relative magnifications (R_{BA}, R_{CA}, R_{DA}) of the components (B, C, D) with respect to component A are shown on Figure 5. F96's observed radio flux density ratios are also shown. The values of R_{BA} are almost the same for all of our models ($R_{BA} \approx 0.88$–0.90), implying that the components B and A change their image magnifications in the same manner as ϵ varies. The values of R_{DA} as a function of ϵ have the largest slope, ranging from ≈ 0.78 to ≈ 1.3. The values of R_{BA} and R_{CA} for all models are within the observational uncertainties. As a result, models of lower and higher ellipticities are not distinguished by R_{BA} and R_{CA} alone. Unlike R_{BA} or R_{CA}, R_{DA} is clearly distinguished by ϵ. For $\epsilon > 0.19$, the values of R_{DA} are within the observational uncertainty of R_{DA}. Thus, models of higher ellipticity are favored by the observational constraint on R_{DA}, although the overall best-fit ellipticity is 0.12.

Since our models are not singular at the center, they can be used to investigate the possibility of a fifth image (i.e., component E) close to the center of the galaxy. For a given ellipticity, component E is brighter for a larger core size (see also Wallington & Narayan 1993). Figure 6 shows how the relative magnification of component E with respect to com-

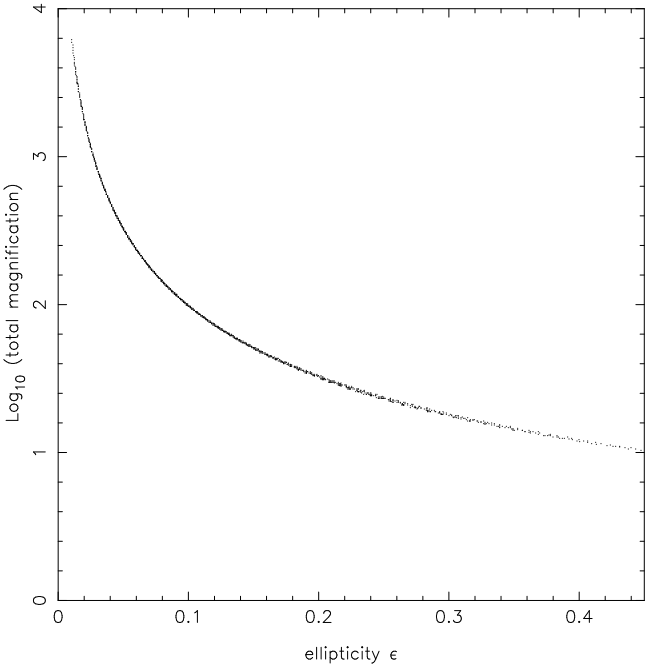

FIG. 4.—Relation between the predicted total image magnification of a model and the ellipticity of the model. Models of lower ellipticity predict larger total magnifications.

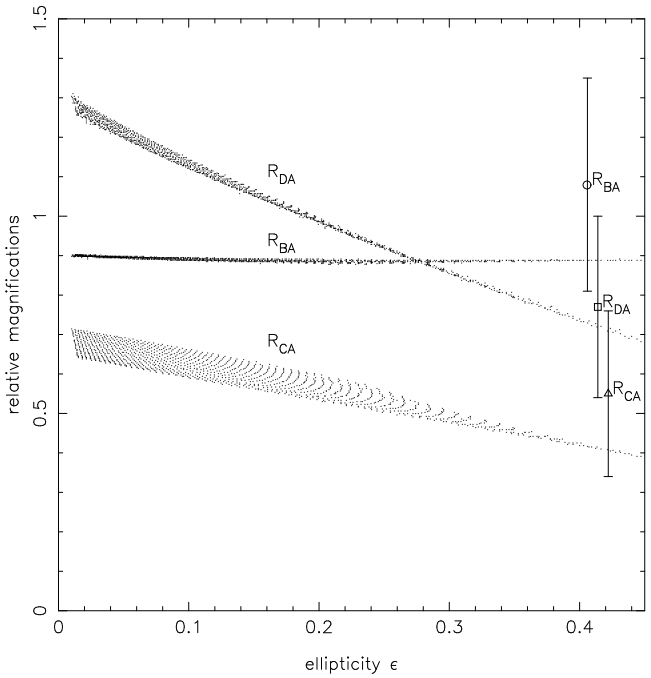

FIG. 5.—Relative magnifications (R_{BA}, R_{CA}, R_{DA}) of the image components (B, C, D) with respect to A depend on the ellipticity ϵ of the model. Models of higher and lower ellipticities are distinguishable by their different predicted values of R_{DA}. F96's measured radio flux density ratios are shown and can be compared to the predicted relative magnifications of our models.

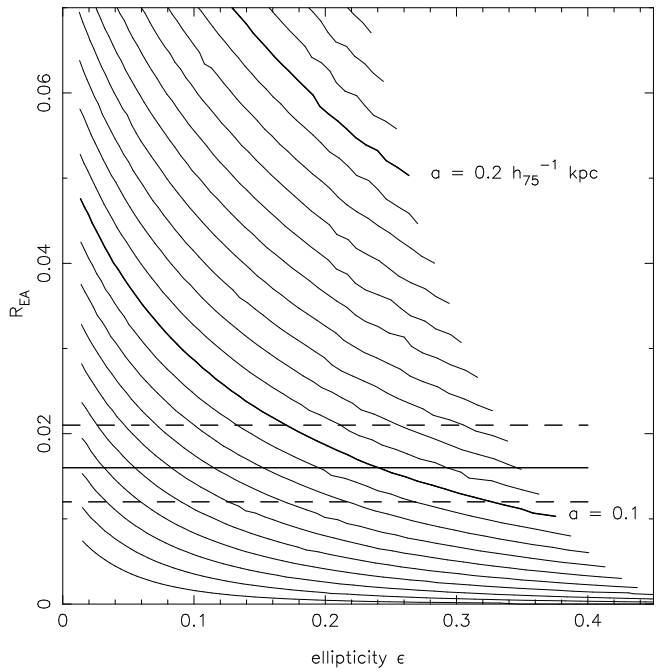

FIG. 6.—Predictions for the relative brightness of image component E (i.e., the fifth image) for various models. Models of larger lens core sizes have brighter fifth images. The horizontal line is the Racine (1991) estimate of R_{EA} based on his CFHT data analysis. The two dashed lines represent the uncertainties.

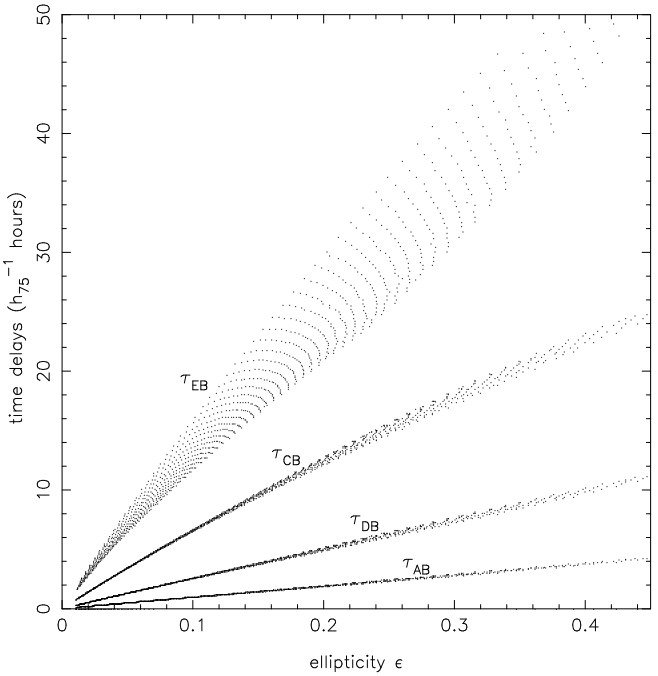

FIG. 7.—Relative time delays (τ_{AB}, τ_{CB}, τ_{DB}, τ_{EB}) of the components (A, C, D, E) with respect to the leading component B. They are well constrained by the model ellipticity. Models of lower ellipticity predict shorter time delays than models of higher ellipticity.

ponent A, R_{EA}, depends on the lens core size and ellipticity. Some of the models predict fifth images bright enough to be tested by future observations. The horizontal line is the Racine (1991) estimate of R_{EA} based on analysis of his CFHT data. The two dashed horizontal lines are the uncertainties. Note that we confined ourselves to $R_{EA} \lesssim 0.07$ following the Rix et al. (1992) upper limit on the relative brightness of the fifth image.

The expected time delays (τ_{AB}, τ_{CB}, τ_{DB}) of the components (A, C, D) with respect to the leading image B are illustrated in Figure 7. The maximum time delay among the bright components, τ_{CB}, ranges from less than 1 h_{75}^{-1} hr to ≈ 20 h_{75}^{-1} hr. We also include the expected time delay of component E, τ_{EB}, with respect to the leading image B, which is the largest time delay.

The shape of the projected mass was determined by ω (recall that we fixed β at 60°), which in turn was constrained by the values chosen for a and v. For either smaller v or larger a, the value of ω minimizing χ^2 was smaller, making ϵ smaller (i.e., making the shape more circular). Since all of the mass (luminous and nonluminous) is assumed to be accounted for by equation (1), ω must be interpreted as an "effective" major-to-minor axis ratio. So if dark matter of lower ellipticity (e.g., $\lesssim 0.1$) is important for lensing, then ω will be different from the luminous mass major-to-minor axis ratio. For all of our models, the mass inside 0.″9 from the center of the galaxy was found to be $(1.48–1.51) \times 10^{10}$ h_{75}^{-1} $M_\odot$, which is in good agreement with both WP94's value of $(1.48 \pm 0.01) \times 10^{10}$ h_{75}^{-1} $M_\odot$ inside θ_E ($\approx$0.″869–0.″876) and the Rix et al. (1992) value of $(1.44 \pm 0.03) \times 10^{10}$ h_{75}^{-1} $M_\odot$ inside 0.″9, which indicates that the determination of the lensing mass is almost independent of the choice of lens models. For our models $\gamma \approx$ 23.°1, which corresponds to a position angle of 66.°9. Finally, it is worth noting that the vertical position of the lens mass center relative to component A was found to be $\approx$0.″927 $\pm$ 0.″001 for all of our models. This value is in between C91's measured value of 0.″936 and the Rix et al. (1992) measured value of 0.″918 (recall that those two groups used the *HST* observations). A sizable fraction of χ^2 ($\approx$4) came from the disagreement between the model lens vertical position and the observed galaxy center vertical position (C91).

4. DISCUSSION AND SUMMARY

Our oblate mass model for the lensing galaxy does better than all previous models in explaining the observed properties of the Einstein Cross. Previous models included the best constant mass-to-light ratio model (Rix et al. 1992) and the best multiparametric model (WP94). The constant mass-to-light ratio model is conceptually simple and directly uses the observed light distribution of the lensing galaxy. Although the constant mass-to-light ratio model qualitatively explained the observed image properties, the disagreement between the positions predicted by the model and the observed image positions is much larger than the observational uncertainty. This implies that the constant mass-to-light ratio model is a fair but not an accurate description of the real lens. Moreover, unless the core size of an isothermal dark matter halo exceeds a few kpc (i.e., a few tens percent of the galactic disk size), we cannot completely neglect the contribution of dark matter to lensing (see Rix et al. 1992). WP94's multiparametric geometrical models used an external shear γ to account for the nonspherical component of the mass distribution. The WP94 models reproduced the observed image positions very accurately (a factor of 3–4 times more accurate than the best constant

mass-to-light ratio models), but their models of weaker and stronger external shears predicted almost indistinguishable relative image magnifications, while predicting very different total magnifications and time delays. Because of this "parameter degeneracy" in predicting relative magnifications, if WP94's predicted relative magnifications are consistent with observations, then all of their models are almost equally acceptable. So the WP94 models cannot constrain the total magnification or time delays. On the other hand, if WP94's predicted relative magnifications are inconsistent with observations, then all of their models must be rejected as a whole as they disagree with observations. This difficulty, arising from the parameter degeneracy in WP94's geometrical models, indicates that the lens astigmatism as adopted by WP94 is not the best method for deriving the physical properties of the Einstein Cross, although such a model can explain the lens geometry fairly accurately.

Our physical lens is an approximation of the three-dimensional mass distribution in the lensing galaxy. Our models reproduce the observed image positions with an accuracy comparable to measurement uncertainties (C91), which is better than all previous models. Our grid of calculated models within the 99% confidence region of parameter space predict a wide range of total magnifications, time delays, and relative magnifications. The grid of models also allows a wide range of ellipticity (see Fig. 3). The elliptical models in the grid are characterized mostly by the ellipticity of the projected mass and are insensitive to the radial index or core size, except that the relative magnification of the fifth image depends on the core size. Models of the same ellipticity predict very similar relative magnifications, total magnification, and time delays regardless of the values of the radial index and core size. On the other hand, models of different ellipticities predict not only different total magnifications and time delays, but also clearly distinguishable relative magnifications. The range of relative magnifications corresponding to the range of ellipticity (Fig. 5) is relatively large. This distinguishable or nondegenerate prediction on the relative magnifications of our oblate mass models for the Einstein Cross should be ascribed to the internal ellipticity inherent to elliptical lenses since this characteristic was not shared by the accurate external shear lens models of WP94. The WP94 geometrical models predict almost indistinguishable or a very narrow range of relative magnifications for different external shear strengths. Therefore, it is almost impossible to distinguish between the external shear models by observing relative magnifications, even though relative magnifications would in principle be easier to observationally determine than the total magnification or time delays. However, the current observational estimate of the relative magnifications (F96) provides only weak model constraints due to the observational uncertainties. Nevertheless, future accurate observational constraints on the relative magnifications can be used to exclude most of our models, thereby offering the possibility of deducing a tightly constrained elliptical lens for the Einstein Cross, assuming that the constrained relative magnifications are within the range of our model predictions (at present, we do not see any reasons why this should not be the case).

This is important for several reasons. First, since relative image magnifications depend mostly on ellipticity, we can constrain the ellipticity by constraining relative magnifications. While the ellipticity of the mass is expected to differ from the ellipticity of the light for the lensing spiral galaxy, it will be interesting to quantify the difference. Secondly, the total image magnification can be constrained naturally as soon as the ellipticity is constrained (see Fig. 4). The determination of total magnification is important for determining the intrinsic luminosity of the QSO, and could be used in conjunction with other observations to probe the physics of QSOs (see Rauch & Blandford 1991; Jaroszyński, Wambsganss, & Paczyński 1992; WP94). Lastly, the predicted time delays can also be constrained when the ellipticity is constrained (see Fig. 7). This can be important because constrained time delays could be used to estimate the Hubble constant with Einstein Cross monitoring. Recall that the ratio of observed time delay to our predicted time delay is simply h_{75}^{-1}, and this result is insensitive to the assumption on the value of the deceleration parameter, q_0, because the lens has such a low redshift. However, two issues must be settled to determine the Hubble constant using the Einstein Cross lens. One is that the expected short time delays ($\lesssim 20\ h_{75}^{-1}$ hr) give rise to observational difficulties. For the detection of time delays, the QSO would need to undergo a noticeable intrinsic variation on a timescale shorter than the time delay, and a closely spaced monitoring program ($\Delta t < 1$ hr) would be required. Nonetheless, the possibility of detecting time delays in the Einstein Cross deserves further consideration because of its importance. The other issue is that the mass distribution of the lensing galaxy must be accurately determined by the observational properties of the lens (i.e., image positions and relative magnifications) in order to predict time delays accurately. In this study we considered mass distributions with elliptical symmetry and found that a range of elliptical mass distributions is consistent with the current observational constraints. While this implies that the considered mass distributions can be a good approximation to the true mass distribution, it also means that the current observational constraints are not strong enough to determine the mass distribution. The agreement between our models and the current observations is so good that it is not very meaningful to consider more sophisticated mass models based only on the current observations. For example, the true mass distribution will not exactly follow elliptical symmetry because the galaxy has a bar. However, the bar is extended far outside and thus should be less important for the lensing. It is likely that more sophisticated mass models would fit the observations somewhat better than our present results, but with more free parameters. More sophisticated mass models will need to be considered only when future observational constraints turn out to be inconsistent with our mass models.

Our grid of models predicts various relative brightnesses for the fifth image: $0 \lesssim R_{\rm EA} \lesssim 0.07$ (see Fig. 6). The quantified relationship between $R_{\rm EA}$ and the lens core size presented here can be used to estimate a lens core size for the Einstein Cross. The determination of the lens core size is of interest because the knowledge of the core size is needed to determine the distribution of mass at the central region of the galaxy.

Presently, both the relative magnifications ($R_{\rm BA}$, $R_{\rm CA}$, $R_{\rm DA}$) of the components (B, C, D) with respect to A and the relative magnification $R_{\rm EA}$ of component E (i.e., the fifth image) with respect to A are poorly constrained. Since the optical images show microlensed variability (e.g., Østensen et al. 1996) and are susceptible to dust extinction from the lensing (spiral) galaxy, unless those two effects are modeled

accurately, the optical image brightness ratios cannot represent the relative macrolensing magnifications. More accurate modeling might be accomplished in the future through the use of results from infrared observations. Currently, measurements of radio flux density ratios are more likely to represent the relative macrolensing magnifications (see F96 and references therein). F96 derived a rough estimate of the relative image magnifications using VLA observations. Nevertheless, to better constrain the lens models of the Einstein Cross, more accurate observations in the radio would be useful. Whatever future observations (e.g., radio, infrared, optical) can be used to better determine the relative macrolensing magnifications, our grid of models can be used to interpret them. Results on the possibility of a fifth image have been reported by Racine (1991) and Rix et al. (1992). While Racine (1991) gave an estimate of $R_{\rm EA}$ using ground-based observations (CFHT), Rix et al. (1992) set an upper limit on $R_{\rm EA}$ using the *HST* Wide Field Camera observations. Our grid of models will be even more useful if more accurate observational constraints on the fifth image can be obtained.

In summary, we presented a large grid of realistic power-law lens models within a 99% confidence region of parameter space around the best model (§ 3). We found that:

1. Our models are in excellent agreement with the observed image positions. They are also consistent with other observables (i.e., relative image magnifications of the bright components and constraints on the fifth component), which, however, are not as well constrained by current observations.

2. Our model grid covers a wide range of relative image magnifications. When the relative magnifications are more accurately determined from future observations, we expect most of our models to be excluded, thereby narrowing the parameter space of the grid.

3. The properties of our basic model (i.e., total magnification, relative magnifications, and time delays) depend mainly on the ellipticity of the projected lens mass. Therefore, if the relative magnifications can be better constrained with future observations, the ellipticity will be well constrained.

4. When the ellipticity is constrained, so is the total magnification. This is important because it should be useful for probing the physics of QSOs through future studies of Q2237+0305.

5. The predictions for time delays are also constrained by the ellipticity. Thus, if someday observations are made that both further constrain our model grid and result in measurable time delays, our grid of models can be used to constrain the Hubble constant, assuming that the true mass distribution is consistent with our model mass distributions.

6. Finally, our model grid covers a range of values for $R_{\rm EA}$. The predictions for $R_{\rm EA}$ can be compared to future observational constraints on $R_{\rm EA}$ that will aid in distinguishing between models (specifically the lens core size).

We are grateful to the anonymous referee for useful comments that improved the manuscript. We thank the editor E. L. Wright for comments on the presentation of the paper. We also thank C. Hazard for motivational comments and D. J. Hillier for comments on numerical codes. K. H. C. thanks J. Busche, J. Herald, R. Kurosawa, L. Lee, and S. Strub for their assistance in the astrophysics computing lab at the University of Pittsburgh.

REFERENCES

Chae, K.-H. 1998, Ph.D. thesis, Univ. Pittsburgh, in preparation
Chae, K.-H., Khersonsky, V. K., & Turnshek, D. A. 1998, ApJ, submitted (CKT)
Crane, P., et al. 1991, ApJ, 369, L59 (C91)
Falco, E. E., Lehár, J., Perley, R. A., Wambsganss, J., & Gorenstein, M. V. 1996, AJ, 112, 897 (F96)
Goldstein, H. 1980, Classical Mechanics (2d ed.; Reading: Addison-Wesley)
Grogin, N. A., & Narayan, R. 1996, ApJ, 464, 92
Huchra, J., et al. 1985, AJ, 90, 691
Jaroszyński, M., Wambsganss, J., & Paczyński, B. 1992, ApJ, 396, L65
Kassiola, A., & Kovner, I. 1993, ApJ, 417, 450
Keeton, C. R., & Kochanek, C. S. 1998, preprint (astro-ph/9705194)
Keeton, C. R., Kochanek, C. S., & Seljak, U. 1997, ApJ, 482, 604
Kent, S. M., & Falco, E. E. 1988, AJ, 96, 1570
Kochanek, C. S. 1991, ApJ, 373, 354
Kochanek, C. S. 1996, ApJ, 473, 595
Kormann, R., Schneider, P., & Bartelmann, M. 1994, A&A, 284, 285
Østensen, R., et al. 1996, A&A, 309, 59
Press, W. H., Teukolsky, S. A., Vetterling, W. T., & Flannery, B. P. 1992, Numerical Recipes (2d ed.; Cambridge: Cambridge Univ. Press)
Racine, R. 1991, AJ, 102, 454
Ratnatunga, K. U., Ostrander, E. J., Griffiths, R. E., & Im, M. 1995, ApJ, 453, L5
Rauch, K. P., & Blandford, R. D. 1991, ApJ, 381, L39
Rix, H.-W., Schneider, D. P., & Bahcall, J. N. 1992, AJ, 104, 959
Schneider, D. P., et al. 1988, AJ, 95, 1619
Turner, E. L., Ostriker, J. P., & Gott, J. R. 1984, ApJ, 284, 1
Wallington, S., & Narayan, R. 1993, ApJ, 403, 517
Wambsganss, J., & Paczyński, B. 1994, AJ, 108, 1156 (WP94)
Yee, H. K. C. 1988, AJ, 95, 1331